Appl. Math. Mech. -Engl. Ed., **39**(11), 1617–1630 (2018)

Applied Mathematics and Mechanics (English Edition)

https://doi.org/10.1007/s10483-018-2390-6

Investigation of generalized Fick's and Fourier's laws in the second-grade fluid flow*

T. HAYAT[1,2], S. AHMAD[1], M. I. KHAN[1,†], A. ALSAEDI[2]

1. Department of Mathematics, Quaid-i-Azam University 45320, Islamabad 44000, Pakistan;
2. Nonlinear Analysis and Applied Mathematics (NAAM) Research Group, Department of Mathematics, Faculty of Science, King Abdulaziz University, Jeddah 21589, Saudi Arabia

(Received May 1, 2018 / Revised Jul. 5, 2018)

Abstract The second-grade fluid flow due to a rotating porous stretchable disk is modeled and analyzed. A porous medium is characterized by the Darcy relation. The heat and mass transport are characterized through Cattaneo-Christov double diffusions. The thermal and solutal stratifications at the surface are also accounted. The relevant nonlinear ordinary differential systems after using appropriate transformations are solved for the solutions with the homotopy analysis method (HAM). The effects of various involved variables on the temperature, velocity, concentration, skin friction, mass transfer rate, and heat transfer rate are discussed through graphs. From the obtained results, decreasing tendencies for the radial, axial, and tangential velocities are observed. Temperature is a decreasing function of the Reynolds number, thermal relaxation parameter, and Prandtl number. Moreover, the mass diffusivity decreases with the Schmidt number.

Key words second-grade liquid, thermal and solutal stratification, Cattaneo-Christov double diffusion, rotating stretchable disk

Chinese Library Classification O361
2010 Mathematics Subject Classification 75A10

1 Introduction

The fluid flow due to rotating disks have numerous applications in many fields, e.g., computer storage devices, rotating machinery, gas or marine turbines, electronic devices, rotating disk reactors for biofuels production, rotating heat exchangers, and medical equipment[1–14]. Karman[1] investigated the hydrodynamic flow by a rotating infinite disk, and developed an appropriate transformation to transform the governing PDEs into ODEs. Reddy et al.[2] studied the heat and mass transport in the MHD flow of copper and silver water due to rotating

* Citation: HAYAT, T., AHMAD, S., KHAN, M. I., and ALSAEDI, A. Investigation of generalized Fick's and Fourier's laws in the second-grade fluid flow. *Applied Mathematics and Mechanics* (*English Edition*), **39**(11), 1617–1630 (2018) https://doi.org/10.1007/s10483-018-2390-6

† Corresponding author, E-mail: mikhan@math.qau.edu.pk

Project supported by the Natural Science and Engineering Research Council (NSERC) of Canada (No. NSERC-RGPIN204992)

porous disks, and implemented the finite element technique. Sheikholeslami et al.[3] explored the nanofluid flow with rotating inclined disks. Turkyilmazoglu[4] evaluated the flow due to rotating disks with nanomaterials. Hayat et al.[5] investigated the viscoelastic nanomaterial convective flow between two stretchable rotating disks. Imtiaz et al.[6] presented the radiative flow of carbon-water nanomaterials between two convectively heated rotating disks. Hayat et al.[7] analyzed the probable error and statistical declaration for the radiative two-phase flow submerged in Ag-H_2O and Cu-H_2O nanoparticals. Takhar et al.[8] presented the steady axisymetric flow between two porous disks.

The stratification in heat and mass transfer arises through the variation of temperature, concentration differences, or the presence of different densities. Double stratification involved various practical applications, e.g., the thermal stratification of reservoirs, oceans, rivers, and ground-water reservoirs, heterogenous mixtures, manufacturing processing, and the density stratification of atmosphere. Srinivasacharya and Surender[15] discussed the significance of doubly stratified laminar flow of a viscous fluid with nanoparticles. Hayat et al.[16] explored the double stratified nanomaterial flow with thixotropic materials in presence of heat source/sink. Babu and Sandeep[17] examined the doubly stratified melting flow in the rate type nanoliquid with heat generation. Nadeem and Muhammad[18] addressed the non-Fourier heat flux and double stratification in the rate type nanoliquid flow over a stretched sheet. Waqas et al.[19] explored the stratified flow of an Oldroyd-B nanofluid in presence of heat generation.

The perception of heat transport is affective in technological and industrial processes. These applications include energy production, atomic reactors cooling, power generation, etc. Due to this fact, many scientists and engineers are interested in analyzing the mechanism of heat transport. Fourier[20] proposed the well-known heat conduction law. Cattaneo[21] modified the Fourier law by adding the time relaxation term. Christov[22] replaced the time derivative by the upper convective derivative in the theory proposed by Cattaneo[23], and names the new theory as the Cattaneo-Christov heat flux theory (generalized Fourier's law). Hayat et al.[24] examined the Cattaneo-Christov relation for heat flux to explore the flow of rate type liquid over a stretchable sheet. Shehzad et al.[25] examined the effects of the non-Fourier heat flux and autocatalysis cubic chemical reaction on viscoelastic fluid flow. Some recent relative contributions to the Cattaneo-Christov theory can be referred to Refs. [26]–[28].

On the basis of the above discussion, in this paper, we aim to discuss the flow of second-grade liquid due to a rotating porous stretchable disk. Second-grade fluid is the principal subclass of differential type fluids. The model proposed by Rivlin and Ericksen[29] can predict the effects of normal stress. It concentrates on the effects of the non-zero and unequal normal stress differences in the shearing flows flagging way for their applicability in various mechanisms such as die swell, rod-climbing, cooling of electronic devices, and solar energy collectors. The Darcy relation is employed for a porous medium. The heat and mass transfer are explored subject to Fourier's and Fick's laws. The thermal and solutal stratifications at the surface are considered. Appropriate transformations are used to obtain the nonlinear systems. The homotopy analysis method (HAM) is utilized to obtained the series solutions of the nonlinear systems[30–39]. The effects of involved variables on the temperature, velocities, concentration, skin frictions, and heat and mass transfer rates are examined.

2 Formulation

Here, the three-dimensional steady incompressible flow of the second-grade fluid due to a rotating porous stretchable disk is discussed. The flow is due to the linear stretching velocity. The energy equation is discussed in the absence of thermal radiation and viscous dissipation. The heat and mass transfer are described by Fourier's and Fick's laws. The disk rotates at $z = 0$ with the angular speed ω and the stretching rate a_1 (in the axial direction, see Fig. 1). Solutal and thermal stratifications are accounted. The relevant expressions are as follows[10,26,40]:

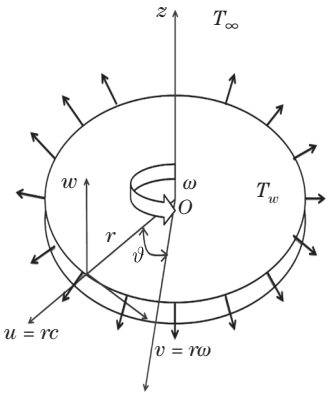

Fig. 1 Schematic diagram (color online)

$$\frac{\partial u}{\partial r}+\frac{\partial w}{\partial z}+\frac{u}{r}=0, \tag{1}$$

$$\begin{aligned}&u\frac{\partial u}{\partial r}-\frac{v^2}{r}+w\frac{\partial u}{\partial z}\\&=\nu\frac{\partial^2 u}{\partial z^2}+\frac{\alpha_1}{\rho}\Big(u\frac{\partial^3 u}{\partial r\partial z^2}+w\frac{\partial^3 u}{\partial z^3}+\frac{\partial v}{\partial r}\frac{\partial^2 v}{\partial z^2}-\frac{v}{r}\frac{\partial^2 v}{\partial z^2}+\frac{\partial v}{\partial z}\frac{\partial^2 v}{\partial r\partial z}\\&\quad+\frac{\partial w}{\partial z}\frac{\partial^2 u}{\partial z^2}+3\frac{\partial u}{\partial z}\frac{\partial^2 u}{\partial r\partial z}+2\frac{\partial u}{\partial r}\frac{\partial^2 u}{\partial z^2}-\frac{1}{r}\Big(\frac{\partial u}{\partial z}\Big)^2\Big)-\frac{\nu}{k^*}u,\end{aligned} \tag{2}$$

$$\begin{aligned}&u\frac{\partial v}{\partial r}+\frac{uv}{r}+w\frac{\partial v}{\partial z}\\&=\nu\frac{\partial^2 v}{\partial z^2}+\frac{\alpha_1}{\rho}\Big(u\frac{\partial^3 v}{\partial r\partial z^2}+w\frac{\partial^3 v}{\partial z^3}-\frac{\partial v}{\partial z}\frac{\partial^2 u}{\partial r\partial z}+\frac{u}{r}\frac{\partial^2 v}{\partial z^2}\\&\quad-\frac{1}{r}\frac{\partial v}{\partial z}\frac{\partial u}{\partial z}\Big)-\frac{\nu}{k^*}v,\end{aligned} \tag{3}$$

$$\rho c_p\Big(u\frac{\partial T}{\partial r}+w\frac{\partial T}{\partial z}\Big)=-\nabla q^\circ, \tag{4}$$

$$\Big(u\frac{\partial C}{\partial r}+w\frac{\partial C}{\partial z}\Big)=-\nabla J^\circ \tag{5}$$

with

$$\begin{cases}u(0)=a_1 r, \quad v(0)=\omega r, \quad w(0)=0, \quad T(0)=T_1=T_0+Ar,\\ C(0)=C_1=C_0+Dr, \quad v(\infty)=0, \quad u(\infty)=0,\\ T(\infty)=T_2=T_0+Br, \quad C(\infty)=C_2=C_0+Er,\end{cases} \tag{6}$$

where u, v, and w indicate the velocity components, ρ indicates the fluid density, ν indicates the kinematic viscosity, α_1 indicates the normal stresses modulus, k^* indicates the porosity permeability, c_p indicates the specific heat, T indicates the temperature, C indicates the concentration, q° indicates the heat flux, and J° indicates the mass flux. With the Cattaneo-Christov theory,

we can express the heat and mass fluxes as follows:

$$q^\circ + \lambda_E\Big(\frac{\partial q^\circ}{\partial t} + V\nabla q^\circ - q^\circ\nabla V + (\nabla V)q^\circ\Big) = -k\nabla T, \tag{7}$$

$$J^\circ + \lambda_C\Big(\frac{\partial J^\circ}{\partial t} + J^\circ\nabla J^\circ - J^\circ\nabla V + (\nabla V)J^\circ\Big) = -D_B\nabla C, \tag{8}$$

where λ_E and λ_C represent the relaxation time of heat and mass, respectively, k represents the thermal conductivity, and D_B represents the mass diffusion coefficient. For steady and incompressible flow, Eqs. (7) and (8) become

$$q^\circ + \lambda_E(V\nabla q^\circ - q^\circ\nabla V) = -k\nabla T, \tag{9}$$

$$J^\circ + \lambda_C(J^\circ\nabla J^\circ - J^\circ\nabla V) = -D_B\nabla C. \tag{10}$$

Eliminating q° and J° from Eqs. (4) and (5) and Eqs. (9) and (10), we have the temperature and concentration equations as follows:

$$\begin{aligned} u\frac{\partial T}{\partial r} + w\frac{\partial T}{\partial z} = \frac{k}{\rho c_p}\Big(\frac{\partial^2 T}{\partial z^2}\Big) - \lambda_E\Big(u^2\frac{\partial^2 T}{\partial r^2} + w^2\frac{\partial^2 T}{\partial z^2} + 2uw\frac{\partial^2 T}{\partial z\partial r} \\ + \Big(u\frac{\partial u}{\partial r} + w\frac{\partial u}{\partial z}\Big)\frac{\partial T}{\partial r} + \Big(u\frac{\partial w}{\partial r} + w\frac{\partial w}{\partial z}\Big)\frac{\partial T}{\partial z}\Big), \end{aligned} \tag{11}$$

$$\begin{aligned} u\frac{\partial C}{\partial r} + w\frac{\partial C}{\partial z} = D_B\Big(\frac{\partial^2 C}{\partial z^2}\Big) - \lambda_C\Big(u^2\frac{\partial^2 C}{\partial r^2} + w^2\frac{\partial^2 C}{\partial z^2} + 2uw\frac{\partial^2 C}{\partial\omega z\partial r} \\ + \Big(u\frac{\partial u}{\partial r} + w\frac{\partial u}{\partial z}\Big)\frac{\partial C}{\partial r} + \Big(u\frac{\partial w}{\partial r} + w\frac{\partial w}{\partial z}\Big)\frac{\partial C}{\partial z}\Big). \end{aligned} \tag{12}$$

We consider[14]

$$\begin{cases} u = r\omega f'(\eta), \quad v = r\omega g(\eta), \quad w = -2h\omega f(\eta), \\ \theta(\eta) = \dfrac{T - T_2}{T_1 - T_0}, \quad \phi(\eta) = \dfrac{C - C_2}{C_1 - C_0}, \quad \eta = \dfrac{z}{h}. \end{cases} \tag{13}$$

Then, Eq. (1) is trivially verified, and we have

$$f''' + \varpi Re(f'f''' - 2ff'''' + 2(f'')^2 + (g')^2) + Re(g^2 + 2ff'' - (f')^2) - \beta Ref' = 0, \tag{14}$$

$$g'' + 2\varpi Re(f'g'' - fg''' - g'f'') - 2Re(f'g - fg') - Re\beta g = 0, \tag{15}$$

$$\theta'' + RePr(2f\theta' - \theta f' - Sf') - \gamma_1 PrRe(4f^2\theta'' + ((f')^2 - 2ff'')(\theta + S)) = 0, \tag{16}$$

$$\phi'' + ReSc(2f\phi' - f'\phi - Zf') - \gamma_2 ScRe(4f^2\phi'' + ((f')^2 - 2ff'')(\phi + Z)) = 0, \tag{17}$$

$$\begin{cases} f(0) = 0, \quad f'(0) = A_1, \quad f'(\infty) = 0, \quad g(0) = 1, \quad g(\infty) = 0, \\ \theta(0) = 1 - S, \quad \theta(\infty) = 0, \quad \phi(0) = 1 - Z, \quad \phi(\infty) = 0, \end{cases} \tag{18}$$

where

$$\begin{cases} Re = \dfrac{\omega h^2}{\nu}, \quad \varpi = \dfrac{\alpha_1}{\rho h^2}, \quad \beta = \dfrac{\nu}{k^*\omega}, \quad Pr = \dfrac{\rho c_p\nu}{k}, \quad Sc = \dfrac{\nu}{D_B}, \\ A_1 = \dfrac{a_1}{\omega}, \quad \gamma_1 = \lambda_E\omega, \quad \gamma_2 = \lambda_C\omega, \quad S = \dfrac{B}{A}, \quad Z = \dfrac{E}{D}. \end{cases} \tag{19}$$

In the above equations, Re represents the Reynolds number, ϖ represents the material parameter, β represents the porosity parameter, Pr represents the Prandtl number, Sc represents the Schmidt number, A_1 represents the disk stretching parameter, γ_1 represents the thermal relaxation, γ_2 represents the concentration relaxation, S represents the thermal stratification, and Z represents the solutal stratification.

Mathematically, the skin friction coefficients C_{f_r} and C_{f_ϑ}, heat transfer rate Nu_r, and mass transfer rate Sh_r are defined as follows:

$$C_{f_r}=\frac{-2\tau_{zr}}{\rho(u_w)^2},\quad C_{f_\vartheta}=\frac{-2\tau_{\vartheta r}}{\rho(v_w)^2},\quad Nu_r=\frac{hq_w}{k(T_1-T_2)},\quad Sh_r=\frac{hJ_w}{D_B(C_1-C_2)},\tag{20}$$

where

$$\begin{cases}\tau_{zr}=\Big(\mu\dfrac{\partial u}{\partial z}+\alpha_1\Big(u\dfrac{\partial^2 u}{\partial r\partial z}+w\dfrac{\partial^2 u}{\partial z^2}+\dfrac{\partial v}{\partial r}\dfrac{\partial v}{\partial z}+2\dfrac{\partial u}{\partial r}\dfrac{\partial u}{\partial z}+\dfrac{v}{r}\dfrac{\partial v}{\partial z}\Big)\Big)_{(z=0)},\\ \tau_{\vartheta r}=\Big(\mu\dfrac{\partial v}{\partial z}+\alpha_1\Big(u\dfrac{\partial^2 v}{\partial r\partial z}+w\dfrac{\partial^2 v}{\partial z^2}-\dfrac{\partial v}{\partial z}\dfrac{\partial w}{\partial z}+\dfrac{u}{r}\dfrac{\partial v}{\partial z}\Big)\Big)_{(z=0)},\\ q_w=-k\Big(\dfrac{\partial T}{\partial z}\Big)_{(z=0)},\quad J_w=-D_B\Big(\dfrac{\partial C}{\partial z}\Big)_{(z=0)}.\end{cases}\tag{21}$$

Substituting Eq. (21) into Eq. (20), we have

$$\begin{cases}C_{f_r}=-\dfrac{2}{(Re_r)A_1^2}(f''(0)+Re\varpi(2g(0)g'(0)-2f(0)f'''(0)+3f'(0)f''(0))),\\ C_{f_\vartheta}=-\dfrac{2}{Re_r}(g'(0)+Re\varpi(4f'(0)g'(0)-2f(0)g''(0))),\\ Nu_r=-\dfrac{\theta'(0)}{1-S},\quad Sh_r=-\dfrac{\phi'(0)}{1-Z},\end{cases}\tag{22}$$

where τ_{zr} and $\tau_{\vartheta r}$ indicate the shear stresses, q_w indicates the heat flux, J_w indicates the mass flux, and $Re_r=\frac{rh\omega}{\nu}$ indicates the local Reynolds number.

3 Series solution

The initial approximations for nonlinear expression and auxiliary linear operators are

$$\begin{cases}f_0(\eta)=A_1-A_1\mathrm{e}^{-\eta},\quad g_0(\eta)=\mathrm{e}^{-\eta},\quad \theta_0(\eta)=\mathrm{e}^{-\eta},\quad \phi_0(\eta)=\mathrm{e}^{-\eta},\\ L_f=\dfrac{\partial^3}{\partial\eta^3}-\dfrac{\partial}{\partial\eta},\quad L_g=\dfrac{\partial^2}{\partial\eta^2}-1,\quad L_\theta=\dfrac{\partial^2}{\partial\eta^2}-1,\quad L_\phi=\dfrac{\partial^2}{\partial\eta^2}-1\end{cases}\tag{23}$$

with

$$\begin{cases}L_f(b_0+b_1\mathrm{e}^{-\eta}+b_2\mathrm{e}^{\eta})=0,\quad L_g(b_3\mathrm{e}^{-\eta}+b_4\mathrm{e}^{\eta})=0,\\ L_\theta(b_5\mathrm{e}^{-\eta}+b_6\mathrm{e}^{\eta})=0,\quad L_\phi(b_7\mathrm{e}^{-\eta}+b_8\mathrm{e}^{\eta})=0,\end{cases}\tag{24}$$

where b_i $(i=0,1,\cdots,8)$ denote the arbitrary constants.

4 Convergence

The auxiliary variables $\hbar_f$, $\hbar_g$, $\hbar_\theta$, and $\hbar_\phi$ have significant roles in controlling and adjusting the convergence region. For the acceptable estimation of such variables, we have $\hbar$-curves at the

40th-order of approximations (see Fig. 2 and Table 1). Figure 2 declares that, the convergence intervals are as follows:

$$-1.6 \leqslant \hbar_f \leqslant -0.5, \quad -1.6 \leqslant \hbar_g \leqslant -0.6, \quad -2.2 \leqslant \hbar_\theta \leqslant -0.7, \quad -1.7 \leqslant \hbar_\phi \leqslant -0.6.$$

Table 1 presents that, the 25th-, 28th-, 22th-, and 30th-orders of deformations are suitable for the convergence to the series solutions for $f''(0)$, $g'(0)$, $\theta'(0)$, and $\phi'(0)$, respectively.

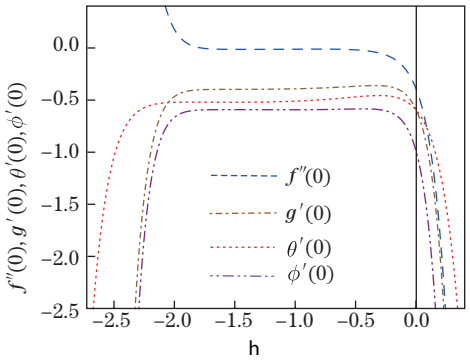

Fig. 2 $\hbar$-curves for $f''(0)$, $g'(0)$, $\theta'(0)$, and $\phi'(0)$

Table 1 Different orders of approximations when $Re = 0.3$, $\varpi = 0.1$, $Pr = 1.5$, $A_1 = \gamma_1 = Z = 0.4$, $\beta = 0.2$, $\gamma_2 = S = 0.5$, and $Sc = 1.0$

Order of approximations	$-f''(0)$	$-g'(0)$	$-\theta'(0)$	$-\phi'(0)$
1	0.142 360	0.649 60	0.550 82	0.345 44
4	0.131 839	0.625 01	0.490 23	0.273 93
8	0.119 088	0.616 75	0.457 00	0.261 50
12	0.022 415	0.599 97	0.566 79	0.284 51
16	0.022 331	0.599 48	0.548 88	0.284 42
20	0.022 224	0.599 18	0.536 61	0.283 84
22	0.022 138	0.599 12	0.536 60	0.283 66
25	0.022 136	0.599 12	0.536 55	0.283 62
28	0.022 133	0.599 12	0.536 52	0.283 62
30	0.022 131	0.599 12	0.536 52	0.283 62
32	0.022 131	0.599 12	0.536 52	0.283 62
36	0.022 131	0.599 12	0.536 52	0.283 62
40	0.022 131	0.599 12	0.536 52	0.283 62

5 Discussion

In this section, we intend to provide the approximate (series) solutions of the resulting systems with the HAM. Here, the effects of different variables on the velocity, concentration, temperature, coefficient of skin friction, temperature gradient, and concentration gradient are physically focused on. Attention is particularly given to the consequences of the Reynolds number Re, porosity parameter β, material parameter ϖ, Prandtl number Pr, thermal relaxation γ_1, solutal relaxation γ_2, stretching parameter A_1, thermal stratification S, and solutal stratification Z.

5.1 Radial, axial, and tangential velocities

Figures 3–13 describe the effects of different physical variables on the radial velocity $f'(\eta)$, axial velocity $f(\eta)$, and tangential velocity $g(\eta)$.

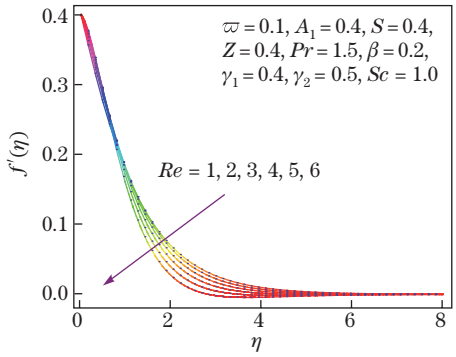

Fig. 3 Effects of Re on $f'(\eta)$

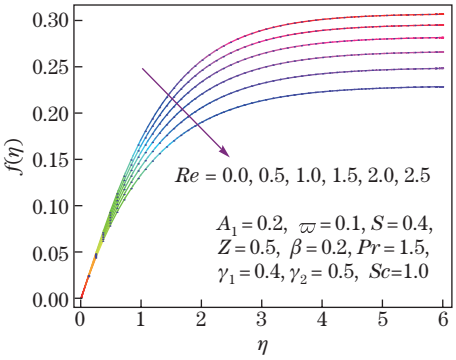

Fig. 4 Effects of Re on $f(\eta)$

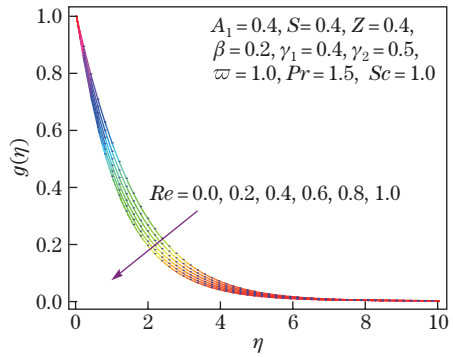

Fig. 5 Effects of Re on $g(\eta)$

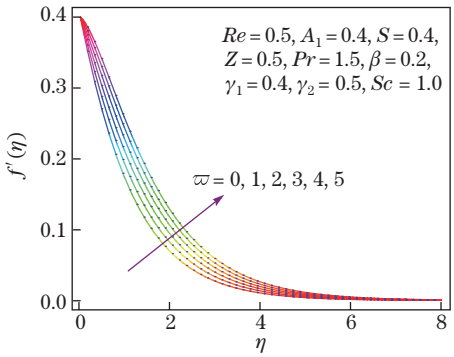

Fig. 6 Effects of ϖ on $f'(\eta)$

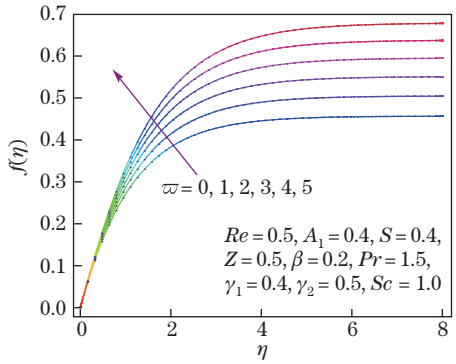

Fig. 7 Effects of ϖ on $f(\eta)$

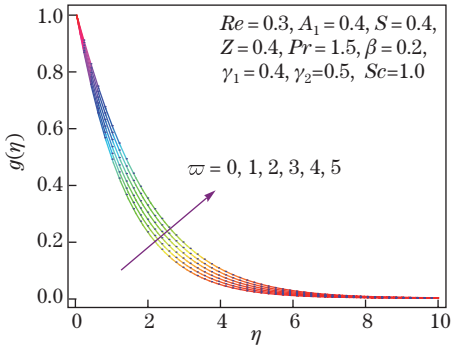

Fig. 8 Effects of ϖ on $g(\eta)$

Figures 3–5 show that the radial $f'(\eta)$, axial $f(\eta)$, and tangential $g(\eta)$ velocities decay for the Reynolds number Re. From the figures, we can see that Re is an increasing function of the angular speed ω, which is responsible for the decay in the fluid velocities.

The effects of the material parameter ϖ on the radial $f'(\eta)$, axial $f(\eta)$, and tangential $g(\eta)$ velocities are portrayed in Figs. 6–8. Clearly, the velocities (radial, axial, and tangential) increase with the material parameter ϖ.

Figures 9–11 sketch the behaviors of the radial $f'(\eta)$, axial $f(\eta)$ and tangential $g(\eta)$ velocities via the porosity parameter β. It is noticed that the velocities $f'(\eta)$, $f(\eta)$, and $g(\eta)$ decay with β.

Figures 12 and 13 are portrayed to show the effects of the parameter A_1 on the axial and

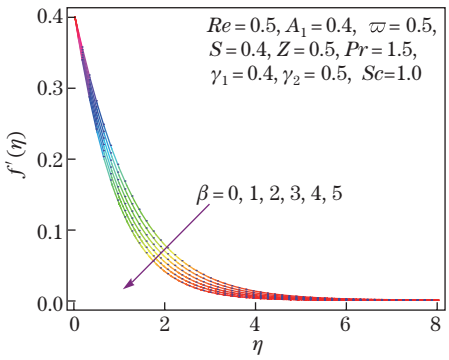

Fig. 9 Effects of β on $f'(\eta)$

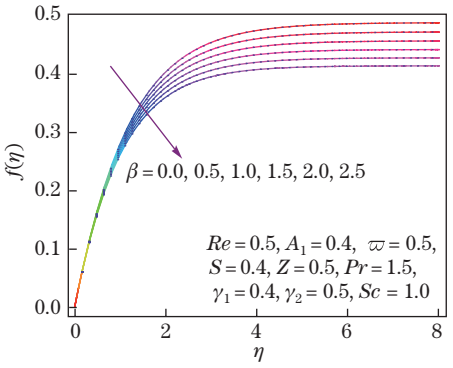

Fig. 10 Effects of β on $f(\eta)$

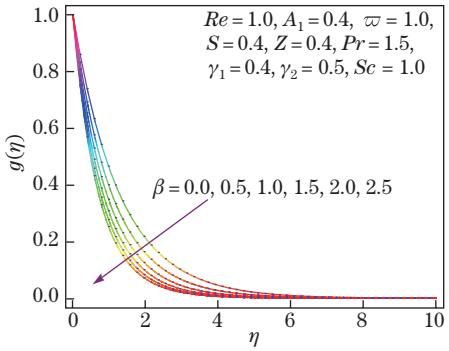

Fig. 11 Effects of β on $g(\eta)$

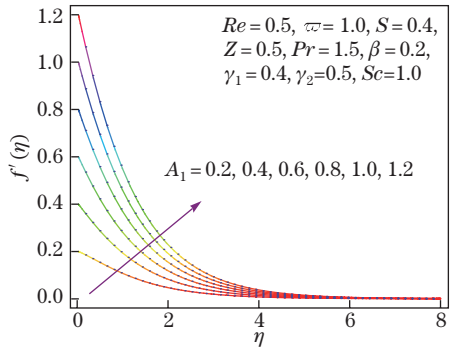

Fig. 12 Effects of A_1 on $f'(\eta)$

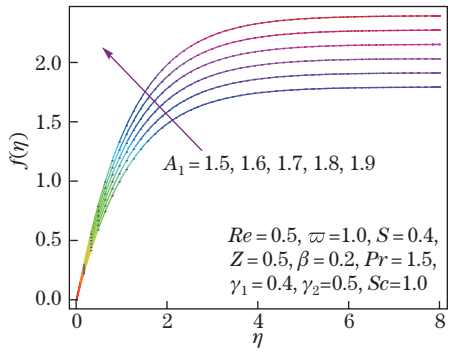

Fig. 13 Effects of A_1 on $f(\eta)$

radial velocities. For larger A_1, the axial and radial velocities are enhanced. This is due to the increase in the stretching rate.

5.2 Temperature profile

Figures 14–17 are displayed to interpret the effects of different parameters on the temperature field $\theta(\eta)$.

Figure 14 is plotted to discuss $\theta(\eta)$ for Pr. From the figure, we can see that the temperature is a decreasing function of Pr. When Pr increases, the thermal conductivity weakens, and therefore $\theta(\eta)$ decays.

Figure 15 is sketched to show the effects of the Reynolds number Re on $\theta(\eta)$. As can be seen in the figure, when the Reynolds number increases, less temperature field can be noticed.

Figure 16 shows the effects of γ_1 on the temperature field. From the figure, we can see that an augmentation in γ_1 indicates a decrease in $\theta(\eta)$. Physically, the material particles need much time to transfer heat to its contiguous particles. Thus, $\theta(\eta)$ is larger for $\gamma_1 = 0$ in case of Fourier's law when compared with non-Fourier's heat flux model.

Figure 17 depicts the behavior of the temperature field via the thermal stratification. From the figure, we can see that temperature is a decreasing function of the thermal stratification parameter. Physically, the difference between the surface temperature and the ambient temperature decreases gradually. As a result, the temperature decreases.

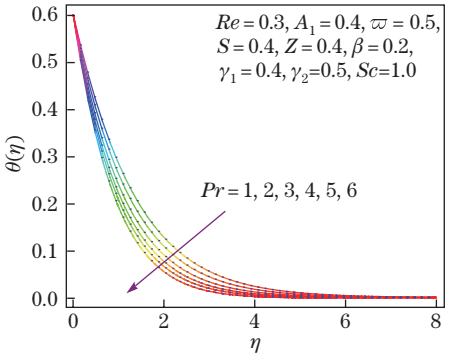

Fig. 14 Effects of Pr on $\theta(\eta)$

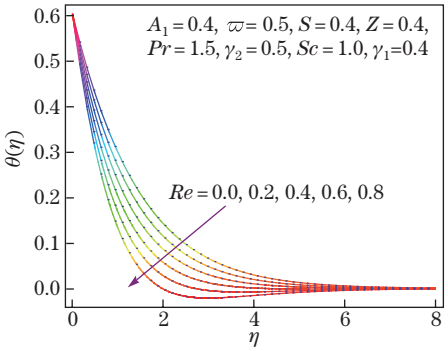

Fig. 15 Effects of Re on $\theta(\eta)$

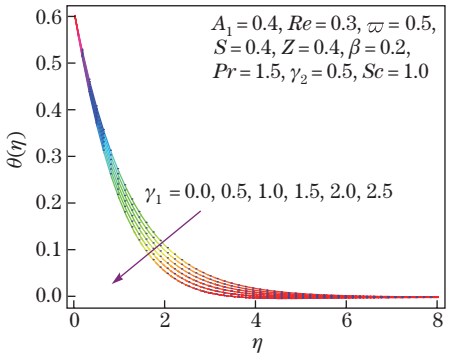

Fig. 16 Effects of γ_1 on $\theta(\eta)$

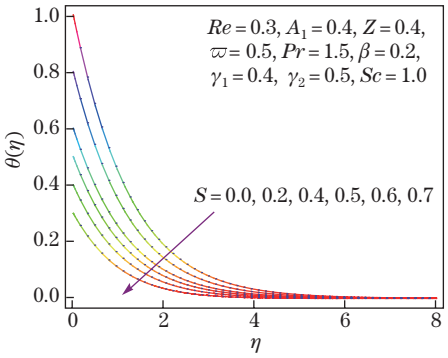

Fig. 17 Effects of S on $\theta(\eta)$

5.3 Concentration profile

Figures 18–21 are sketched to analyze the effects of the Reynolds number, Schmidt number, concentration relaxation, and solutal stratification on the concentration field.

The effects of the Reynolds number Re on the concentration field $\phi(\eta)$ is shown in Fig. 18. From the figure, we can see that the concentration decays for the Reynolds number.

Figure 19 is sketched for the concentration field via the Schmidt number. It shows a decreasing behavior of concentration for the Schmidt number. Since the Schmidt number is the ratio of momentum to mass diffusivity and the mass diffusivity decays for larger Schmidt numbers, the concentration field decays when the Schmidt number increases.

Figures 20 and 21 show the effects of the concentration relaxation and solutal stratifications on $\phi(\eta)$. From the figures, we can see that when the concentration relaxation variable γ_2

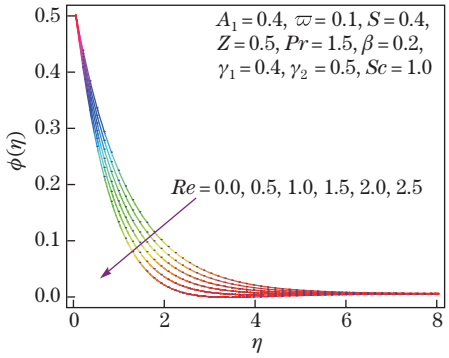

Fig. 18 Effects of Re on $\phi(\eta)$

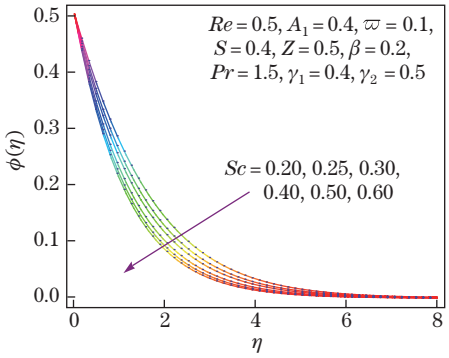

Fig. 19 Effects of Sc on $\phi(\eta)$

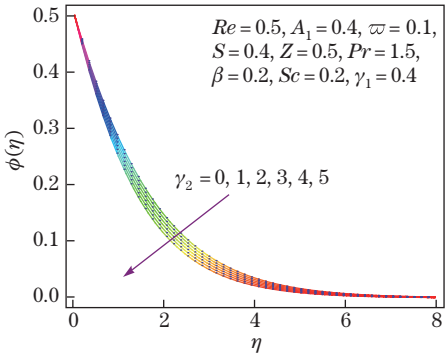

Fig. 20 Effects of γ_2 on $\phi(\eta)$

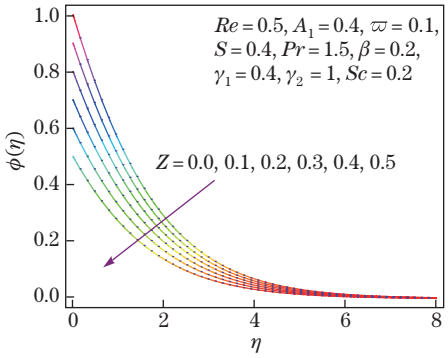

Fig. 21 Effects of Z on $\phi(\eta)$

increases, the concentration field decays. A similar behavior is observed for the solutal stratification variable (see Fig. 21). This is because that the concentration difference diminishes between the surface and the ambient fluid.

5.4 Velocity, temperature, and concentration gradients

Figures 22–31 are portrayed to reveal the effects of different involved variables, e.g., the Reynolds number, material parameter, porosity parameter, Prandtl number, thermal relaxation, thermal stratification, Schmidt number, concentration relaxation, and solutal stratification on

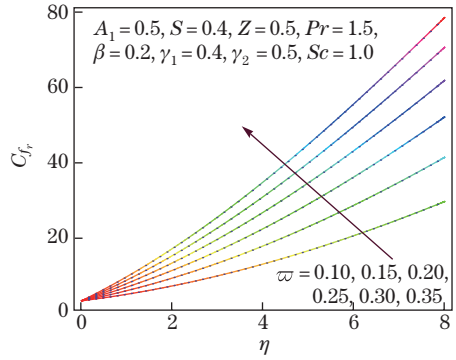

Fig. 22 Variations of C_{f_r} via Re and ϖ

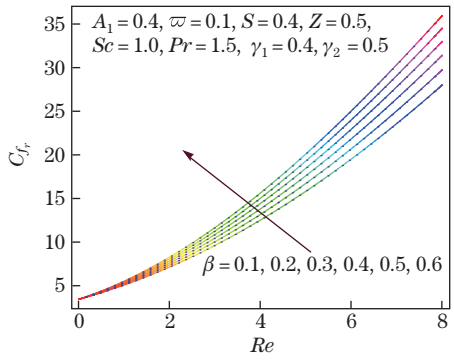

Fig. 23 Variations of C_{f_r} via Re and β

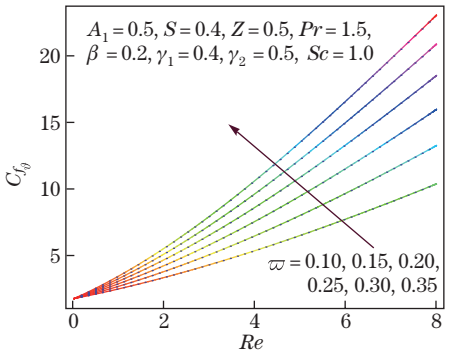

Fig. 24 Variations of C_{f_ϑ} via Re and ϖ

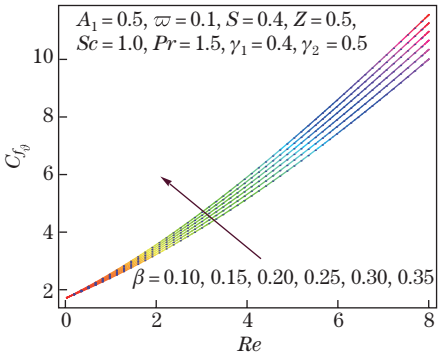

Fig. 25 Variations of C_{f_ϑ} via Re and β

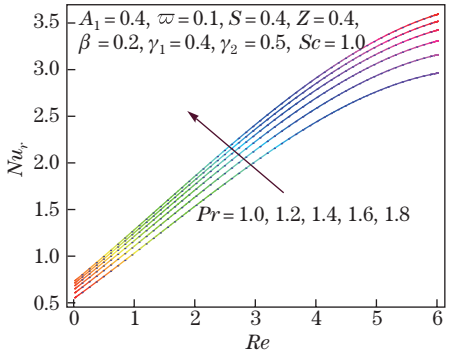

Fig. 26 Variations of Nu_r via Re and Pr

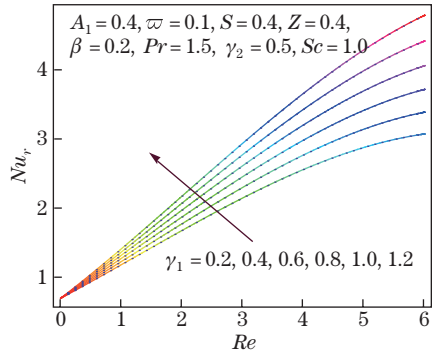

Fig. 27 Variations of Nu_r via Re and γ_1

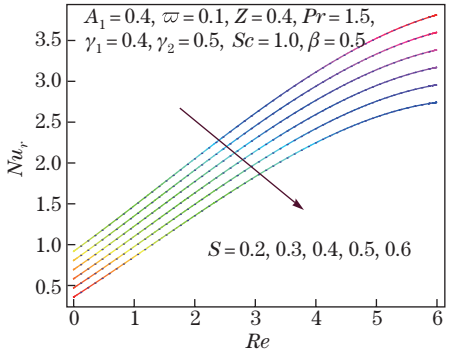

Fig. 28 Variations of Nu_r via Re and S

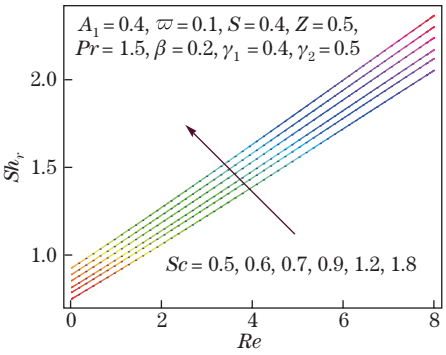

Fig. 29 Variations of Sh_r via Re and Sc

the skin friction coefficients and heat and mass transfer rates. From the figure, we can see that, the surface drag force is an increasing function of the Reynolds number, porosity parameter, and material parameter. Similarly, the heat transfer rate enhances for larger Reynolds numbers, Prandtl numbers, and thermal relaxation variables while decreases for fixed values of the thermal stratification variable. Moreover, the mass transfer rate increases for larger Schmidt numbers and solutal stratification and concentration relaxation variables.

6 Concluding remarks

The second-grade fluid flow due to a rotating stretchable disk in a porous medium is investigated. The main concluding remarks are listed as follows:

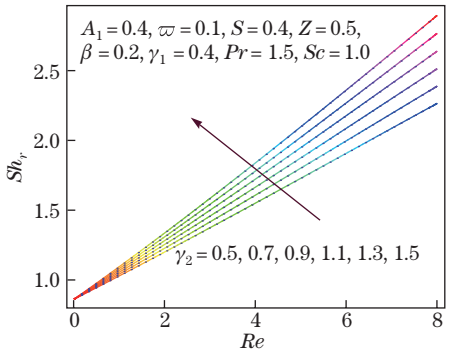

Fig. 30 Variations of Sh_r via Re and γ_2

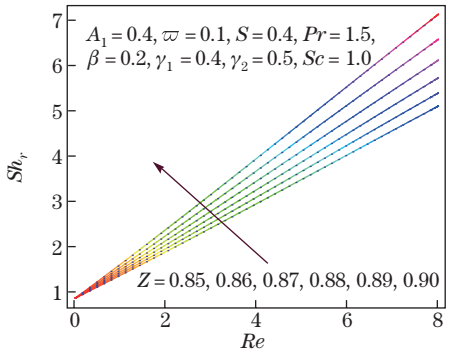

Fig. 31 Variations of Sh_r via Re and Z

(i) The radial velocity increases with ϖ and A_1 while decays with Re and β.

(ii) The axial velocity boosts via Re, ϖ, and A_1 whereas decays with β.

(iii) The tangential velocity enhances for larger ϖ while reduces for larger Re and β.

(iv) The elevation in Pr, Re, γ_1, and S correspond to smaller temperature.

(v) Concentration decays with Re, Sc, γ_2, and Z.

(vi) The temperature gradient enhances for larger ϖ and β.

(vii) The velocity gradient is higher when Re, Pr, and γ_1 are larger, while is smaller when S is larger.

(viii) The Sherwood number boosts via Re, Sc, γ_2, and Z.

References

[1] KARMAN, T. V. Uber laminare und turbulente reibung. *Journal of Applied Mathematics and Mechanics*, **1**, 233–252 (1921)

[2] REDDY, P. S., SREEDEVI, P., and CHAMKHA, A. J. MHD boundary layer flow, heat and mass transfer analysis over a rotating disk through porous medium saturated by Cu-water and Ag-water nanofluid with chemical reaction. *Powder Technology*, **307**, 46–55 (2017)

[3] SHEIKHOLESLAMI, M., HATAMI, M., and GANJI, D. D. Numerical investigation of nanofluid spraying on an inclined rotating disk for cooling process. *Journal of Molecular Liquids*, **211**, 577–583 (2015)

[4] TURKYILMAZOGLU, M. Nanofluid flow and heat transfer due to a rotating disk. *Computer and Fluids*, **94**, 139–146 (2014)

[5] HAYAT, T., JAVED, M., IMTIAZ, M., and ALSAEDI, A. Convective flow of Jeffrey nanofluid due to two stretchable rotating disks. *Journal of Molecular Liquids*, **240**, 291–302 (2017)

[6] IMTIAZ, M., HAYAT, T., ALSAEDI, A., and AHMAD, B. Convective flow of carbon nanotubes between rotating stretchable disks with thermal radiation effects. *International Journal of Heat and Mass Transfer*, **101**, 948–957 (2016)

[7] HAYAT, T., QAYYUM, S., KHAN, M. I., and ALSAEDI, A. Current progresses about probable error and statistical declaration for relitive two phase flow using Ag-H_2O and Cu-H_2O nanomaterials. *International Journal of Hydrogen Energy*, **42**, 29107–29120 (2017)

[8] TAKHAR, H. S., BHARGAVA, R., AGRAWAL, R. S., and BALAJI, A. V. S. Finite element solution of micropolar fluid flow and heat transfer between two porous discs. *International Journal of Engineering Science*, **38**, 1907–1922 (2000)

[9] KHAN, M. I., WAQAS, M., HAYAT, T., and ALSAEDI, A. A comparative study of Casson fluid with homogeneous-heterogeneous reactions. *Journal of Colloid and Interface Science*, **498**, 85–90 (2017)

[10] KHAN, M. I., WAQAS, M., HAYAT, T., KHAN, M. I., and ALSAEDI, A. Behavior of stratification phenomenon in flow of Maxwell nanomaterial with motile gyrotactic microorganisms in the presence of magnetic field. *International Journal of Mechanical Sciences*, **132**, 426–434 (2017)

[11] KHAN, M. I., WAQAS, M., HAYAT, T., ALSAEDI, A., and KHAN, M. I. Significance of nonlinear radiation in mixed convection flow of magneto Walter-B nanoliquid. *International Journal of Hydrogen Energy*, **42**, 26408–26416 (2017)

[12] AZIZ, A., ALSAEDI, A., MUHAMMAD, T., and HAYAT, T. Numerical study for heat generation/absorption in flow of nanofluid by a rotating disk. *Results in Physics*, **8**, 785–792 (2018)

[13] HAYAT, T., HAIDER, F., MUHAMMAD, T., and ALSAEDI, A. On Darcy-Forchheimer flow of carbon nanotubes due to a rotating disk. *International Journal of Heat and Mass Transfer*, **112**, 248–254 (2017)

[14] HAYAT, T., MUHAMMAD, T., SHEHZAD, S. A., and ALSAEDI, A. On magnetohydrodynamic flow of nanofluid due to a rotating disk with slip effect: a numerical study. *Computer Methods in Applied Mechanics and Engineering*, **315**, 467–477 (2017)

[15] SRINIVASACHARYA, D. and SURENDER, O. Effect of double stratification on mixed convection boundary layer flow of a nanofluid past a vertical plate in a porous medium. *Applied Nanoscience*, **5**, 29–38 (2015)

[16] HAYAT, T., WAQAS, M., KHAN, M. I., and ALSAEDI, A. Analysis of thixotropic nanomaterial in a doubly stratified medium considering magnetic field effects. *International Journal of Heat and Mass Transfer*, **102**, 1123–1129 (2016)

[17] BABU, M. J. and SANDEEP, N. UCM flow across a melting surface in the presence of double stratification and cross-diffusion effects. *Journal of Molecular Liquids*, **232**, 27–35 (2017)

[18] NADEEM, S. and MUHAMMAD, N. Impact of stratification and Cattaneo-Christov heat flux in the flow saturated with porous medium. *Journal of Molecular Liquids*, **224**, 423–430 (2016)

[19] WAQAS, M., KHAN, M. I., HAYAT, T., and ALSAEDI, A. Stratified flow of an Oldroyd-B nanoliquid with heat generation. *Results in Physics*, **7**, 2489–2496 (2017)

[20] FOURIER, J. B. J. *Théorie Analytique De La Chaleur*, Cambridge University Press, Cambridge (1822)

[21] CATTANEO, C. *Sulla Conduzione Del Calore*, Springer, Berlin Heidelberg (1948)

[22] CHRISTOV, C. I. On frame indifferent formulation of the Maxwell-Cattaneo model of finite-speed heat conduction. *Mechanics Research Communications*, **36**, 481–486 (2009)

[23] HAYAT, T., FAROOQ, T., ALSAEDI, A., and AL-SOLAMY, F. Impact of Cattaneo-Christov heat flux in the flow over a stretching sheet with variable thickness. *AIP Advances*, **5**, 087159 (2015)

[24] HAYAT, T., QAYYUM, S., IMTIAZ, M., and ALSAEDI, A. Impact of Cattaneo-Christov heat flux in Jeffrey fluid flow with homogeneous-heterogeneous reactions. *PloS One*, **11**, e0148662(2016)

[25] SHEHZAD, S. A., ABBASI, F. M., HAYAT, T., and AHMAD, B. Cattaneo-Christov heat flux model for third-grade fluid flow towards exponentially stretching sheet. *Applied Mathematics and Mechanics* (*English Edition*), **37**(6), 761–768 (2016) https://doi.org/10.1007/s10483-016-2088-6

[26] HAYAT, T., AYUB, T., MUHAMMAD, T., and ALSAEDI, A. Flow of variable thermal conductivity Oldroyd-B fluid with generalized Fourier's and Fick's laws. *Journal of Molecular Liquids*, **234**, 9–17 (2017)

[27] HAYAT, T., KHAN, M. I., FAROOQ, M., ALSAEDI, A., WAQAS, M., and YASMEEN, T. Impact of Cattaneo-Christov heat flux model in flow of variable thermal conductivity fluid over a variable thicked surface. *International Journal of Heat and Mass Transfer*, **99**, 702–710 (2016)

[28] MERAJ, M. A., SHEHZAD, S. A., HAYAT, T., ABBASI, F. M., and ALSAEDI, A. Darcy-Forchheimer flow of variable conductivity Jeffrey liquid with Cattaneo-Christov heat flux theory. *Applied Mathematics and Mechanics* (*English Edition*), **38**(4), 557–566 (2017) https://doi.org/10.1007/s10483-017-2188-6

[29] RIVLIN, R. S. and ERICKSEN, J. L. Stress deformation relations for isotropic materials. *Journal of Rational Mechanics and Analysis*, **4**, 323–425 (1955)

[30] WAQAS, M., KHAN, M. I., HAYAT, T., ALSAEDI, A., and KHAN, M. I. Nonlinear thermal radiation in flow induced by a slendering surface accounting thermophoresis and Brownian diffusion. *The European Physical Journal Plus*, **132**, 280 (2017)

[31] KHAN, M. I., WAQAS, M., HAYAT, T., and ALSAEDI, A. Chemically reactive flow of micropolar fluid accounting viscous dissipation and Joule heating. *Results in Physics*, **7**, 3706–3715 (2017)

[32] HAYAT, T., KHAN, M. I., FAROOQ, M., YASMEEN, T., and ALSAEDI, A. Water-carbon nanofluid flow with variable heat flux by a thin needle. *Journal of Molecular Liquids*, **224**, 786–791 (2016)

[33] KHAN, M. I., HAYAT, T., KHAN, M. I., and ALSAEDI, A. A modified homogeneous-heterogeneous reactions for MHD stagnation flow with viscous dissipation and Joule heating. *International Journal of Heat and Mass Transfer*, **113**, 310–317 (2017)

[34] HAYAT, T., WAQAS, M., KHAN, M. I., and ALSAEDI, A. Analysis of thixotropic nanomaterial in a doubly stratified medium considering magnetic field effects. *International Journal of Heat and Mass Transfer*, **102**, 1123–1129 (2016)

[35] ZHAO, Q., XU, H., TAO, L., RAEES, A., and SUN, Q. Three-dimensional free bio-convection of nanofluid near stagnation point on general curved isothermal surface. *Applied Mathematics and Mechanics* (*English Edition*), **37**(4), 417–432 (2016) https://doi.org/10.1007/s10483-016-2046-9

[36] HAYAT, T., MAKHDOOM, S., AWAIS, SALEEM, S., and RASHIDI, M. M. Axisymmetric Powell-Eyring fluid flow with convective boundary condition: optimal analysis. *Applied Mathematics and Mechanics* (*English Edition*), **37**(7), 919–928 (2016) https://doi.org/10.1007/s10483-016-2093-9

[37] HAYAT, T., AHMAD, S., KHAN, M. I., ALSAEDI, A., and WAQAS, M. Investigation of second-grade fluid through temperature dependent thermal conductivity and non-Fourier heat flux. *Results in Physics*, **9**, 871–878 (2018)

[38] ZHU, J., WANG, S., ZHENG, L., and ZHANG, X. Heat transfer of nanofluids considering nanoparticle migration and second-order slip velocity. *Applied Mathematics and Mechanics* (*English Edition*), **38**(1), 125–136 (2017) https://doi.org/10.1007/s10483-017-2155-6

[39] HAYAT, T., AHMAD, S., KHAN, M. I., and ALSAEDI, A. Modeling and analyzing flow of third grade nanofluid due to rotating stretchable disk with chemical reaction and heat source. *Physica B*: *Condensed Matter*, **537**, 116–126 (2018)

[40] HAYAT,T., QAYYUM, S., ALSAEDI, A., and AHMAD, B. Significant consequences of heat generation/absorption and homogeneous-heterogeneous reactions in second-grade fluid due to rotating disk. *Results in Physics*, **8**, 223–230 (2018)